Structure of Aggregates of *trans*-4-Alkoxy-4′-carboxystilbenes in the Solid State and in Microheterogeneous Media. A Link between the "Unit Aggregate" and Extended Arrays

Shai Vaday, H. Cristina Geiger, Brian Cleary, Jerry Perlstein,* and David G. Whitten*

Department of Chemistry and NSF Center for Photoinduced Charge Transfer, University of Rochester, Rochester, New York 14627

Received: August 13, 1996; In Final Form: October 28, 1996[⊗]

Crystals of three 4-alkoxy-4′-carboxy *trans*-stilbene (ACS) derivatives and a crystal of 4-methoxy-4′-methanoate *trans*-stilbene have been shown to have structures in which the amphiphilic aromatics are arranged in layers remarkably similar to deposited Langmuir−Blodgett multilayer assemblies. Within each layer there is either a glide or pseudoglide (or herringbone) arrangement of the chromophores very similar to that deduced from physical properties and simulations for structurally related stilbene, azobenzene, and tolan amphiphiles in microheterogeneous media, solution, and Langmuir−Blodgett (LB) films. The fluorescence of the crystals is very similar to that associated with LB films of a water-insoluble amphiphilic ACS that is associated with the aggregate. An analysis of the crystal structure indicates that energetically favorable aromatic−aromatic (edge−face) interaction determines the packing within a layer.

Introduction

The formation of small aggregates as relatively stable "supramolecular" entities in microheterogeneous media and in some cases even in solution in arrested crystallization processes has been observed for a wide variety of dyes and aromatic molecules.[1−4] Relatively small aggregation numbers—typically 3 or 4 or a multiple thereof—are indicated for several of these species, and it is indicated that in several cases the aggregate may be a chiral structure. Monte Carlo simulations on monolayer clusters suggest that the stable structure may be a cyclic array or "pinwheel", which when extended results in a glide or herringbone lattice. From the physical properties of these aggregates it appears that favorable nonbonding interactions between π systems may be important forces favoring aggregation and controlling the structure, although other factors such as hydrophobic or solvophobic interactions may also play key roles. Very similar structures have been indicated thus far for aggregates of chromophores as diverse as *trans*-stilbenes,[5] *trans*-azobenzenes,[6] squaraines,[7] diphenylacetylenes,[8] and biphenyls.[9] For Langmuir−Blodgett (LB) films and phospholipid bilayers we have obtained indications that the most important noncovalent interactions occur within a tetramer cluster and thus that extended arrays of these chromophores may be reasonably described as mosaics of the "unit" aggregates.[10] An important question is whether these "unit" aggregates may also be the key intermediates in crystal formation. To address this question, we have recently synthesized and studied crystals of the amphiphilic stilbenes **1**−**3** and **5** (see Scheme 1). We report here a study of these stilbenes and a water-insoluble amphiphilic derivative of closely related structure (**4**) in the solid state, solution, and LB films. The results indicate that these stilbenes form crystals that are indeed extensions of the unit aggregate structure proposed for similar compounds in microheterogeneous media. The crystal structure of **5** (the methyl ester of **1**), a similar amphiphile that cannot form intermolecular hydrogen bonds, was also determined and found to be similar to the structures of **1**−**3**. An evaluation of these crystal structures indicates that edge-to-face nonbonding interactions play a major role in stabilizing the crystals of all four compounds. Similarities between the photophysical properties of **1**−**3** in the crystal and **4** in microheterogeneous media provide additional evidence to provide a link between the supramolecular unit aggregate in solution and the extended structure in the solid state.

Synthesis. All glassware was dried overnight in the oven, except for that used in the saponification reaction. All solvents are reagent grade. Methylene chloride and tetrahydrofuran were distilled over calcium hydride and sodium with benzophenone, respectively. The progress of the reaction and the purity of the final products were monitored by thin layer chromatography (TLC) using chromatogram sheets made of silica gel adsorbent with a fluorescent indicator. The compounds were characterized by nuclear magnetic resonance (NMR) spectra obtained on a GE QE-300 instrument at 300 Mhz for proton.

Synthesis of 4-Ethoxy-4′-carboxylic Acid trans-Stilbene. Methyl 4-methylbenzoate (5.0 g, 33.3 mmol), dry carbon tetrachloride (200 mL), and recrystallized *N*-bromosuccinimide (6.5 g, 36.7 mmol) were placed in a 500 mL two-neck round bottom flask fitted with a reflux condenser. The reaction mixture was refluxed under a nitrogen atmosphere for 5 min, and then a sunlamp (visible light excitation) was used to initiate the reaction. After completion of the reaction (the solution became clear) the mixture was cooled to room temperature, the succinimide was filtered, and the solvent was removed from the filtrate. The crude product was purified by recrystallization with tetrahydrofuran/hexane. The white crystals obtained were dried under a vacuum desiccator. The yield was 70%, 5.3 g.

The Wittig reaction was accomplished by dissolving the dry bromoester (1.0 g, 4.4 mmol) and triphenylphosphine (1.95 g, 7.4 mmol) in dry xylene (110 mL). The flask was purged with nitrogen, and the reaction mixture was refluxed overnight. The Wittig salt formed was filtered, and after recrystallization with chloroform/benzene 1.92 g (90% yield) of product was obtained. One gram (2 mmol) of Wittig salt was dissolved in 30 mL of dry, freshly distilled tetrahydrofuran and 20 mL of methylene chloride. K_2CO_3, 1.4 g (10 mmol), was added followed by ∼10 mg of 18-crown-6. After stirring this mixture for a few minutes, 0.46 g (3 mmol) of 4-ethoxybenzaldehyde was added slowly. The reaction mixture was refluxed overnight, and the progress was monitored by TLC, using hexane/acetone (4:1) as eluent. Unreacted K_2CO_3 was removed by filtration, and the solvent

[⊗] Abstract published in *Advance ACS Abstracts,* December 15, 1996.

S1089-5647(96)02440-6 CCC: $14.00

SCHEME 1

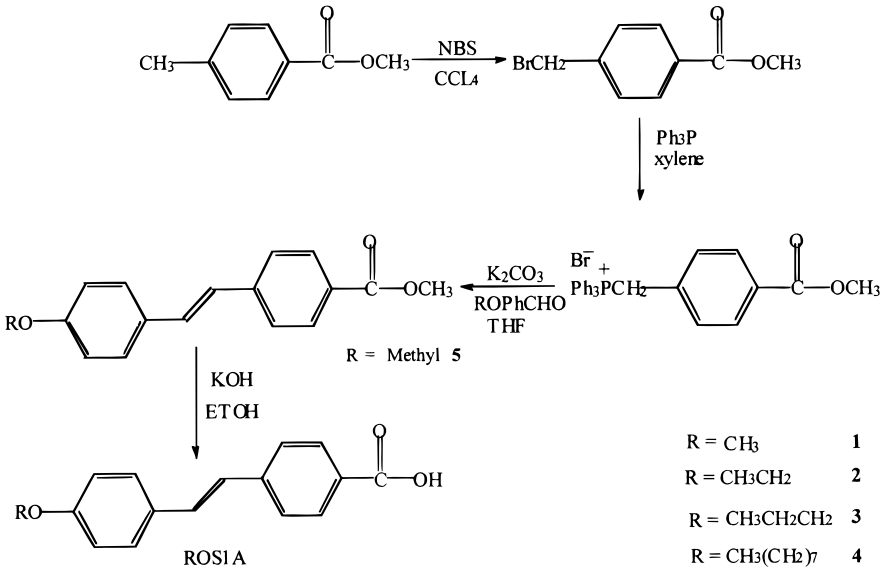

was removed from the filtrate by rotary evaporation. The crude product was purified by silica gel column chromatography using hexane/chloroform (1:1) as eluent. The solid obtained was recrystallized with THF/hexane. White crystals, 0.367 g (64% yield), were obtained.

The stilbene keto ester (0.240 g, 0.85 mmol) was dissolved in 40 mL of ethanol. KOH, 0.190 g (3.4 mmol), was dissolved in 10 mL of water and added to the ethanolic solution. The reaction mixture was refluxed and its progress followed by TLC. After completion of the reaction, about 1 h, 10% hydrochloric acid was added until the solution was acidic to pH paper. The precipitate formed was filtered and recrystallized twice with ethanol/water, affording 0.192 g, 84% yield of acid: mp = 270−275 °C; ^{1}H NMR (DMSO) δ 1.32−1.38 (3H, t, *CH*$_3$-CH$_2$-O-Ar), 4.02−4.10 (2H, quartet, CH$_3$-*CH*$_2$-O-Ar), 6.98 (2H, d, Ar-H), 7.12−7.22 (1H, d, vinylic proton), 7.3−7.4 (1H, d, vinylic proton), 7.68 (2H, d, Ar-H), 7.92 (2H, d, Ar-H). Elemental analysis: calculated for $C_{17}H_{16}O_3$, C 76.09, H 6.01; found, C 75.53, H 5.39.

The procedures used for the synthesis of MeOS1A (**1**) and PrOS1A (**3**) were similar to that described above for the preparation of EtOS1A (**2**).

MeOS1A: mp = 250−255 °C; ^{1}H NMR (DMSO) δ 3.80 (3H, s, CH$_3$O-), 6.95 (2H, d, Ar-H), 7.08−7.18 (1H, d, vinylic proton), 7.24−7.34 (1H, d, vinylic proton), 7.56 (4H, dd, Ar-H), 7.86 (2H, d, Ar-H). Elemental analysis: calculated for $C_{16}H_{14}O_3$, C 75.56, H 5.55; found, C 75.27, H 5.05.

PrOS1A: mp = 290−295 °C; ^{1}H NMR (DMSO) δ 0.92−1.02 (3H, t, *CH*$_3$-CH$_2$-CH$_2$-O), 1.66−1.78 (2H, m, CH$_3$-*CH*$_2$-CH$_2$-O), 3.90−3.98 (2H, t, CH$_3$-CH$_2$-*CH*$_2$-O), 6.93 (2H, d, Ar-H), 7.10−7.20 (1H, d, vinylic proton), 7.29−7.39 (1H, d, vinylic proton), 7.60 (2H, d, Ar-H), 7.90 (2H, d, Ar-H). Elemental analysis: calculated for $C_{18}H_{18}O_3$, C 76.56, H 6.43; found, C 76.08, H 6.23.

Monolayer Experiments. A typical procedure for recording isotherms and deposition of monolayers was as follows. Stock solution concentrations of surfactants were typically 1.4 mg/mL in chloroform (HPLC grade). The subphase used in all studies consisted of Milli-Q water (obtained by passing deionized water through a milli-RO 10 Reverse Osmosis/Milli-Q UF Plus System, specific resistivity 18.2 MΩ) containing 3×10^{-4} MCdCl$_2$ and 5×10^{-5} M NaHCO$_3$ (pH 6.6−6.8). A stock solution of surfactant (200 μL) was spread on the subphase surface in a KSV 5000 trough and the chloroform removed by allowing an evaporation period of 5−10 min prior to compression. The monolayer was then compressed at a speed of 10 mm/min. Deposition was at a surface pressure of 20 mN/m onto quartz slides.

Fluorescence and Absorption Spectra. Fluorescence excitation and emission spectra were recorded on a SPEX 111 CM spectrofluorimeter, with a Xe light source. Absorption spectra were recorded on a Hewlett-Packard diode array spectrophotometer.

Crystal Growing, Data Collection, Structure Solution, and Refinement. Colorless crystals of **2** were grown from a saturated solution in methylene chloride/methanol, powdered **2** was placed in a vial, and 1 mL of methylene chloride was added to the vial. The solution was heated gently, methanol was added until no solid was seen, and the vial was left at ambient temperature in a cupped vial. Similar conditions were used to grow crystals of **1**, **3**, and **5**. Diffraction measurements for **2** and **3** were made on an Enraf-Nonius CAD4 diffractometer with graphite-monochromated Mo Kα radiation operating in the $\omega/2\theta$ scan mode. The cell constants and orientation matrix for data collection were obtained from a least-squares refinement using the setting angles of 25 carefully centered reflections. Diffraction measurements for **1** and **5** were made on a Siemen SMART area detector. The structures of all the crystals were solved by direct methods (SAPI 90, SAPI 91) and expanded using Fourier techniques. Structures were refined by the full-matrix least-squares method. All non-hydrogen atoms were refined anisotropically. Hydrogen atoms were located from difference maps or placed in calculated positions with B_{iso} equivalent to $1.2B_{iso}$ of the bonded non-hydrogen atom. For **2** and **3** an empirical absorption correction, using the program DIFABS, was applied.[11] For **1** and **5** Psi-scan absorption was used using SHELXA program. Neutral atom scattering factors were taken from Cromer and Waber.[12] Anomalous dispersion effects were included in F_{calc}; the values for $\Delta f'$ and $\Delta f''$ were those of Cromer.[13] All calculations were performed using TEXSAN software.[14]

Data collection for **2** was initiated at −30 °C. Of the 5233 data collected, 4813 were unique. Representative reflections showed no decay during acquisition, indicating crystal stability. The final cycle of full-marix least-squares refinement was based on 1626 observed reflections ($I > 3.00\sigma(I)$) and 379 variable parameters and converged with unweighted and weighted agreement factors of $R = \sum||F_o| - |F_c||/\sum|F_o| = 0.054$ and R_w

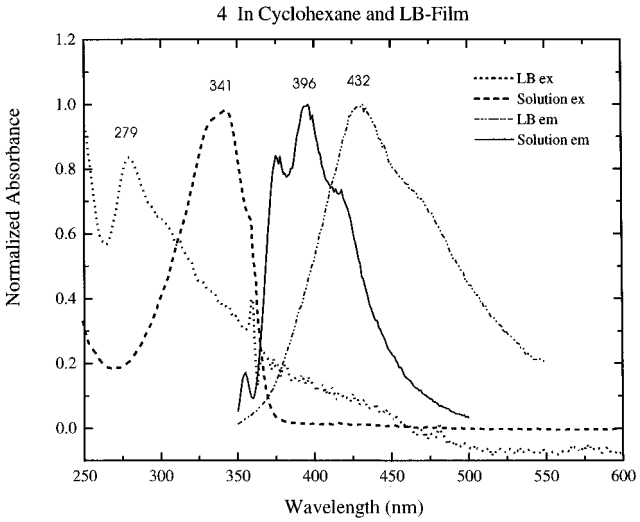

Figure 1. Absorption and emission spectra of **4** (80S1A) in dilute solution of cyclohexane and one-layer LB-film.

$= [(\sum w(|F_o| - |F_c|)^2/wF_o^2)]^{1/2} = 0.056$ with a maximum shift/esd of 0.007. The maximum and minimum peaks on the final difference Fourier map corresponded to 0.24 and -0.22 e$^-$/Å^3, respectively. Data collection for **3** was started at -20 °C. Of the 2972 data collected, 2774 were unique. Representative reflections showed no decay during acquisition, indicating crystal stability. The final cycle of full-matrix least-squares refinement was based on 1424 observed reflections ($I > 3.00\sigma(I)$) and 282 variable parameters and converged with unweighted and weighted agreement factors of $R = 0.044$ and $R_w = 0.044$ with a maximum shift/esd of 0.00. The maximum and minimum peaks on the final difference Fourier map corresponded to 0.24 and -0.22 e$^-$/Å^3, respectively. Data collection for **1** was at -50 °C. Of the 10 279 data collected, 2233 were unique. Representative reflections showed no decay during acquisition, thus indicating crystal stability. The final cycle of full-matrix least-squares refinement was based on 1272 observed reflections ($I > 3.00\sigma(I)$) and 211 variable parameters and converged with unweighted and weighted agreement factors of $R = 0.057$ and $R_w = 0.055$ with a maximum shift/esd of 0.04. The maximum and minimum peaks on the final difference Fourier map corresponded to 0.22 and -0.32 e$^-$/Å^3, respectively. Data collection for **5** was at -50 °C. Of the 8446 data collected, 1943 were unique. Representative reflections again showed no decay during acquisition, indicating crystal stability. The final cycle of full-matrix least-squares refinement was based on 1255 observed reflections ($I > 3.00\sigma(I)$) and 224 variable parameters and converged with unweighted and weighted agreement factors of $R = 0.050$ and $R_w = 0.056$ with a maximum shift/esd of 0.06. The maximum and minimum peaks on the final difference Fourier map corresponded to 0.17 and -0.31 e$^-$/Å^3, respectively. Atomic coordinates for all atoms, bond lengths and angles, anisotropic displacement parameters, torsion angles, and least-squares planes are included as Supporting Information.

Results

Amphiphilic *trans*-4-alkoxy-4′-carboxystilbenes (ACSs) have been found to exhibit aggregation behavior in Langmuir−Blodgett (LB) films similar to that observed with the more widely studied *trans*-stilbene fatty acids (SFAs).[15] Most notably the absorption spectra of supported multilayers prepared from pure ACS or mixtures of ACSs with saturated fatty acids show similar blue shifts, while the fluorescence spectra are red-shifted and characterized by relatively long fluorescence lifetimes.

TABLE 1: Summary of Crystallographic Data for $C_{16}O_3H_{14}$ (1), $C_{17}O_3H_{16}$ (2), and $C_{18}O_3H_{18}$ (3)

empirical formula	$C_{16}O_3H_{14}$	$C_{17}O_3H_{16}$	$C_{18}O_3H_{18}$
crystal size, mm	0.04 × 0.11 × 0.16	0.08 × 0.34 × 0.45	0.15 × 0.60 × 0.60
crystal system	orthorhombic	triclinic	monoclinic
space group	*Pbca* (no. 61)	$P\bar{1}$ (no. 2)	*P*21/*a* (no. 14)
Z	8	4	4
a, Å	56.956(5)	7.082(4)	8.126(5)
b, Å	7.335(2)	7.660(4)	7.467(2)
c, Å	6.183(2)	25.657(5)	24.260(7)
α, deg		92.34(3)	
β, deg		95.74(3)	97.60(4)
γ, deg		98.90(4)	
V, Å^3	2583.3(9)	1365.8(9)	1459.0(9)
d_{calc}, g/cm^3	1.31	1.30	1.29
T, °C	−50	−30	−20
melting point, °C	250	270	280
$\lambda_{Mo\ K\alpha}$ (graphite monochromated)	0.710 69	0.710 69	0.710 69
R^a	0.057	0.054	0.044
R_w	0.055	0.056	0.044

^{a} $R = \sum||F_o| - |F_c||/\sum|F_o|$, $R_w = [(\sum w(|F_o| - |F_c|)^2/wF_o^2)]^{1/2}$.

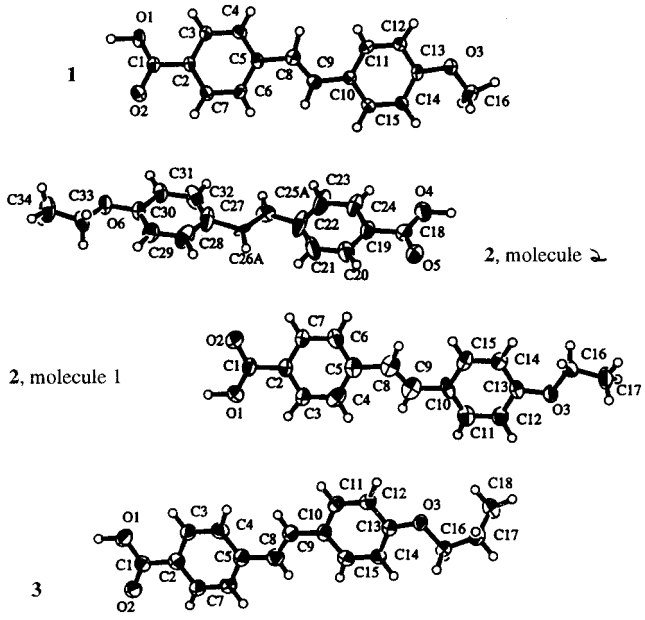

Figure 2. Asymmetric unit of **1**−**3** showing the atom numbering of the atoms. **1** and **3** both have one molecule in the asymmetric unit, while **2** has two molecules in the asymmetric unit.

Figure 1 compares absorption and fluorescence spectra of **4** in dilute solution and in a supported LB film. While neither the SFAs or long-chain ACS amphiphiles such as **4** form crystals suitable for X-ray diffraction studies, the shorter chain ACS amphiphiles **1**−**3** were found to grow suitable crystals from mixtures of solvents such as methanol/methylene chloride. The crystals of **2** grown from a methanol/methylene chloride mixture formed thin plates, resulting from fast growth in two dimensions and slow growth in the third. Examination under a microscope indicated a line through the diagonal of the plate characteristic of "twinning". Each crystal appeared to be two triangular crystals attached together along one side, the twin plane. For X-ray diffraction studies of the crystals of **2** a corner of the twinned crystal was removed and cut into a small segment, making sure that the segment was not twinned. Crystals of **1** and **3** were single crystals with no indication of twinning.

Crystal data for **1**−**3** are summarized in Table 1 (a more detailed table is included as supporting information). Although some individual differences exist for the three compounds, there is a general similarity both in terms of the structures of the

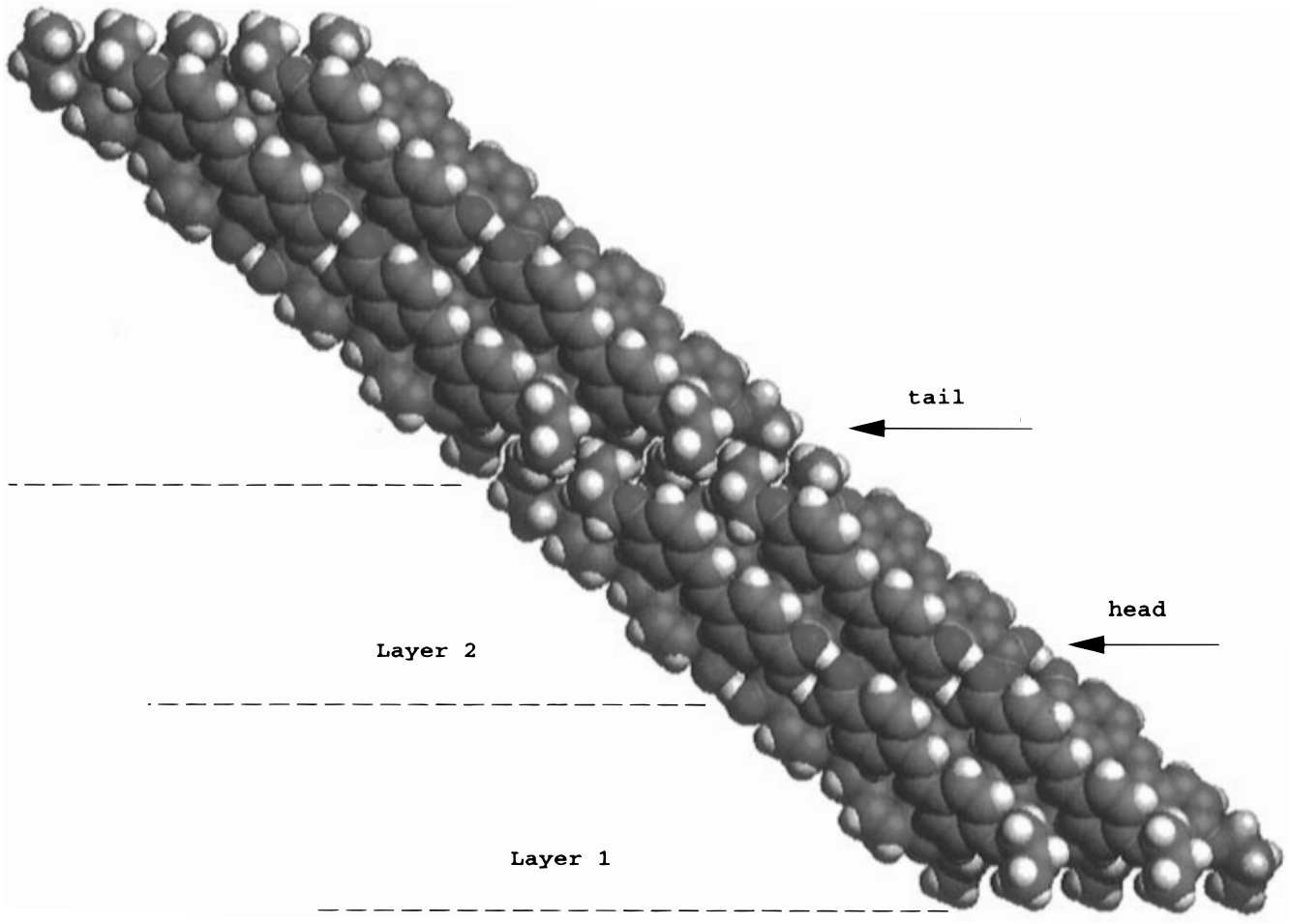

Figure 3. Crystal structure of **3**, a layered structure, with head−head and tail−tail arrangement. The tilt angle of the stilbenes with respect to the layer normal is 48.22°.

individual molecules and the relationships between neighboring molecules in the crystals of all three compounds. Thus the individual molecules show some deviation from planarity with the phenyls twisted at an angle of 3−12°. Similar deviations have been found for crystals of *trans*-stilbene in earlier investigations.[16] The structures of the individual molecules are shown in Figure 2. **1** and **3** both have one molecule in the asymmetric unit, while **2** crystallized with two molecules in the asymmetric unit. The two molecules have a pseudoglide symmetry relationship; that is, the two molecules are packed in an edge-to-face orientation having a T-shape, or herringbone pattern, with an angle of 60° between the planes of the rings (we further explore this in the Discussion section).

When solving the structure of **2**, one molecule in the asymmetric unit showed an orientational disorder. The relative population was determined to be 40:60%. After accounting for the disorder the *R* value decreased significantly, which further supports a disordered structure.

The most striking feature to emerge from the structures obtained for the three ACSs is that the molecules exist in the crystals in layers essentially identical to the structures anticipated for Y-deposited LB multilayers. That is, the molecules of **1**−**3** exist as layers, in each case, in which the molecules have a head−head arrangement such that one face of the layer is characterized by the carboxyl groups of individual ACS molecules, while the other face consists of the corresponding alkoxy groups. This structure is essentially what one would expect for an LB film at the air−water interface. In the extended structure there is contact alternating between the carboxy faces of adjacent layers and between the alkoxy faces (Figure 3). Although small differences exist for the structures of **1**−**3**, in each case, within a single "monolayer" in the crystal the individual molecules are arranged in a "glide" or herringbone lattice, as shown in Figure 4. To further examine the role of aromatic−aromatic interaction in determining the crystal structure, the methyl ester derivative of **1**, **5**, was examined. The crystal structure of **5** is similar to that of **1** except for the layer−layer interaction.

The crystals of **1**−**3** all show fluorescence ranging from 427 to 447 nm, strongly red-shifted from the solution spectrum in methylcyclohexane, but very similar in both wavelength and structure to that observed from **4** and **3** in LB multilayers. Although **3** forms "transient" LB films at the air−water interface both pure and in mixtures with stearic acid, these are unstable over periods of minutes under compression (ca. 20 mN/m), presumably due to the slight solubility of the ACS in water. When a mixed film of **3** with stearic acid is prepared with a large excess of stearic acid (1:5), a film stable enough to be transferred onto a quartz slide is obtained. The photophysical properties of the transferred film are similar to those of **4**. (The organic solution spectra of **1**−**5** are also nearly identical to those shown in Figure 1.) Thus it is reasonable to use water-insoluble **4** as a probe of the likely behavior of **1**−**3** in LB films and supported assemblies. Comparison of **3** in solution LB-film and solid shows a clear trend in fluorescence from the blue spectrum in the dilute monomeric solution to the red-shifted spectrum of the two-dimensional LB-film and to the further red shifted three-dimensional crystal. **1**−**3** have virtually identical absorption, excitation, and emission spectra in solution, yet the crystals all have distinct fluorescence (Figure 5).

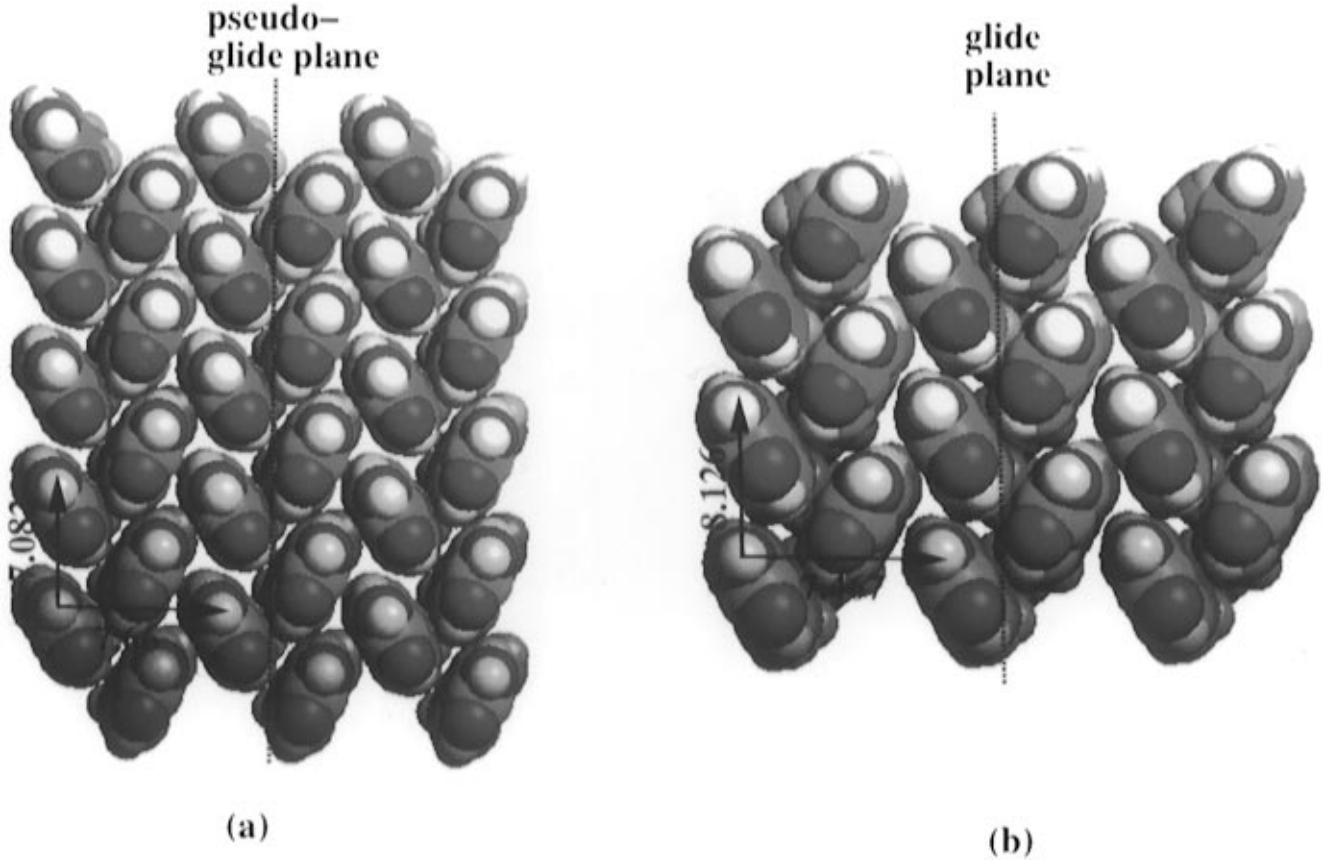

Figure 4. KAP stage 2 analysis showing the layer structure of **2** and **3** each with two repeat vectors. Oxygen atoms in red. (a) The layered stucture of **2** consists of a stage 1 chain of stage 0 dimers repeatedly translated every 7.66 Å to produce the layer. The layer is shown tilted 41.18° with respect to the surface normal. (b) The true glide layer of **3**. The layer is constructed by repeatedly translating a stage 1 glide chain every 7.467 Å. The layer is shown tilted 48.22° with respect to the surface normal.

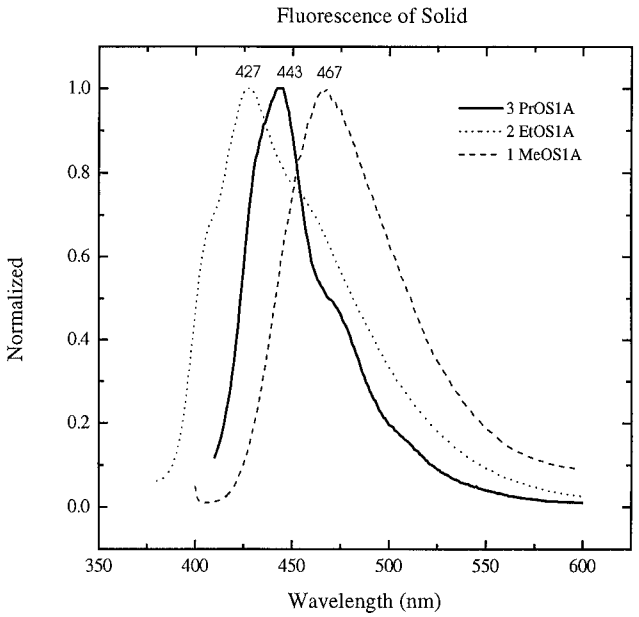

Figure 5. Fluorescence spectra of solids **1**−**3** showing the differences in λ_{max} for the three crystals.

TABLE 2: Analysis of Translation Distances and Emission Maxima for 1−4

compound	translation in X^a	translation in Y^b	λ_{max} emission (nm)
crystal of **1**	6.18	7.34	467
crystal of **3**	8.13	7.47	443
crystal of **2**	7.08	7.66	427
LB-film of **4**			432

[a] *X* is equivalent to the repeat distance along the *a* unit axis for **2** and **3** and to *c* for **1**. [b] *Y* is equivalent to the repeat distance along the *b* unit axis for all three.

TABLE 3. KAP Analysis for 3 Using the CFF91 Force Field (Energy in kcal/mol)

stage	VDW[a]	VDW-(H-bond)[b]	Coulomb[c]	total energy[d]	description
0					only 1 molecule
1	−16.01	0	−2.05	−18.06	glide chain; no H-bond
2	−26.83	0	−2.98	−29.81	glide layer; no H-bond
3	−33.78	+4.96	−12.91	−41.73	*P*21/*a*; H-bond present
Δ(3−2)[e]	−6.95	+4.96	−9.93	−11.92	

[a] Nonbonded van der Waals energy contribution to eq 3. [b] Carboxyl H atom nonbonded energy contribution to eq 3. [c] Electrostatic energy contribution to eq 3. [d] Sum of energy terms (columns 2, 3, and 4). [e] Energy difference between stage 3 and stage 2.

Discussion

The crystal structures determined for **1**−**3** show remarkable congruence with the previously determined simulated structures for monolayer clusters of SFAs.[17] Figure 4 compares an "overhead" view of one layer of **2** with that of **3**. The "pinwheel" tetramer proposed for the "unit aggregate" of several stilbenes and related molecules is easily identifiable in both structures. Interestingly, when the earlier determined crystal structure of *trans*-stilbene is examined, it may be seen that an essentially identical arrangement of the stilbene chromophores exists, and the overall crystal structure is similar to those of **1**−**3**. As will be shown below, this is in agreement with the likelihood that aromatic−aromatic interactions play a major role in determining the crystal structure.

Molecular interactions in the crystal structures of **2** and **3** have been analyzed in terms of Kitaigorodskii's Aufbau

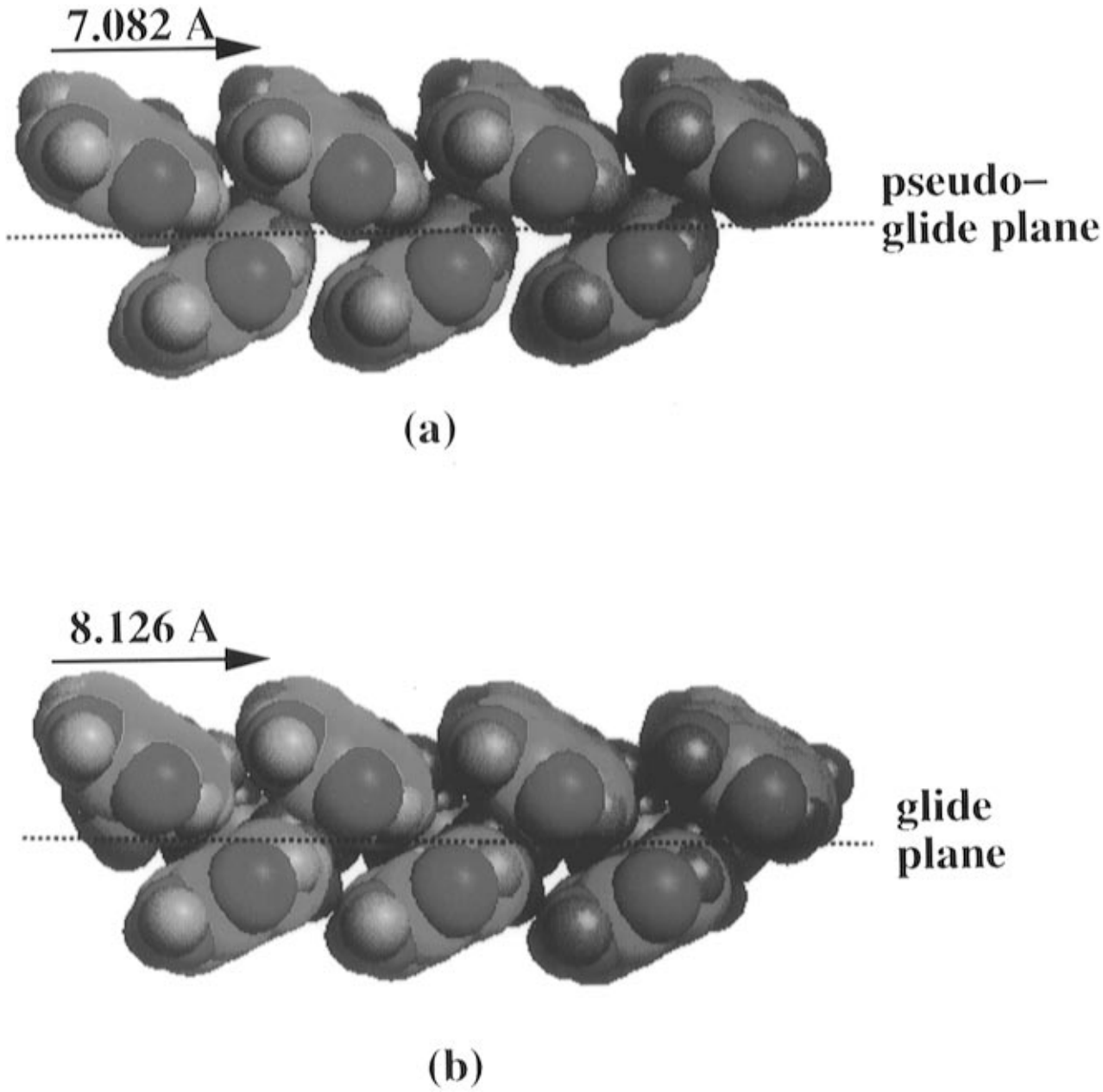

Figure 6. KAP stage 1 lowest energy chain structures for **2** and **3**. View is looking down the long axis of the molecules with oxygen atoms in red. (a) The chain structure of **2** consists of a translation of dimers that have pseudoglide symmetry along the *a*-axis of the unit cell. (b) The true glide chain structure for **3**. Note the structural similarity between these two chains even though they are derived from different space groups.

principle (KAP)[18] using the CFF91 force field from Biosym/MSI.[19] While the two crystal structures have different space groups ($P\bar{1}$ for **2** and $P2_1/a$ for **3**) and differing numbers of molecules in the asymmetric units (2 for **2** and 1 for **3**), the analysis using KAP indicates considerable similarity between the molecular interactions in the two structures. In the KAP analysis we evaluate a crystal structure as composed of a series of substructures, each of which is a local energy minimum of the molecular interaction potential, as evaluated by the force field.[20a] There are four stages in KAP. Stage 0 is represented by the asymmetric units that make up the crystal structure, typically one molecule as for **3** but two molecules for **2**. Stage 1 is the one-domensional chain obtained by the infinite repetition of the stage 0 structure and is thus characterized by a single repeat vector.[20b] For **2** this is a translation chain of the asymmetric unit (Figure 6), whereas for **3** this is a glide chain. Stage 2 is a monolayer obtained by the infinite repetition of stage 1 chains characterized by two repeat vectors, as shown in Figure 4. For **2** this is a translation layer, whereas for **3** it is a glide layer. Finally stage 3 of KAP is the infinite repetition of stage 2 layers characterized by three repeat vectors. This yields the $P\bar{1}$ crystal structure of **2** and the $P2_1/a$ structure of **3**. (For further details about the energy calculations see the Appendix.)

TABLE 4: KAP Analysis for 2 Using the CFF91 Force Field (Energy in kcal/mol)

stage	VDW[a]	VDW-(H-bond)[b]	Coulomb[c]	total energy[d]	
0	−9.18	0	−1.74	−10.92	dimer; no H-bond
1	−15.56	0	−2.78	−18.34	translation chain of dimers; no H-bond
2	−26.37	0	−3.88	−30.25	translation layer of dimers; no H-bond
3	−32.29	+6.02	−13.46	−39.74	$P\bar{1}$; H-bond present
Δ(3−2)[e]	−5.92	+6.02	−9.58	−9.49	

[a] For stage 0 energy computed from eq 3 without dividing by 2. For other stages nonbonded van der Waals energy contribution to eq 3. [b] Carboxyl H atom nonbonded energy contribution to eq 3. [c] Electrostatic energy contribution to eq 3. [d] Sum of energy terms (columns 2, 3, and 4). [e] Energy difference between stage 3 and stage 2.

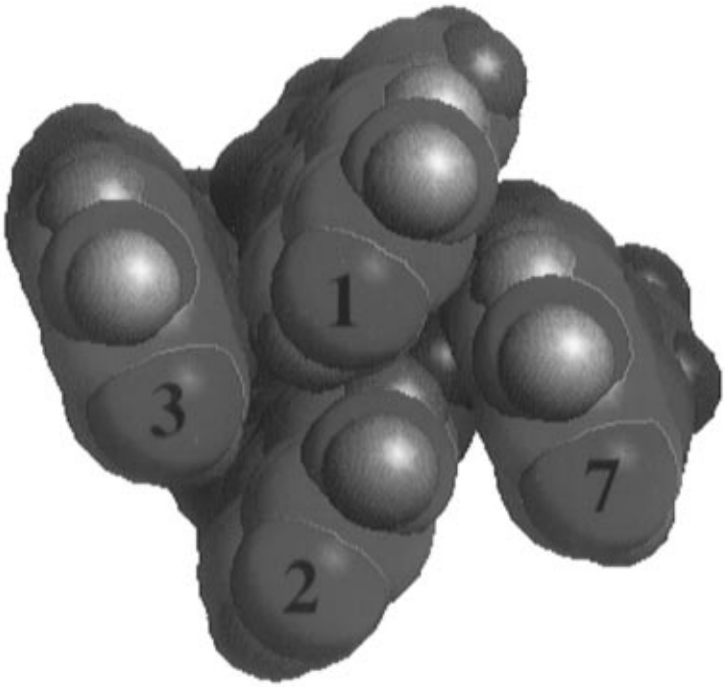

Lowest Energy Tetramer

Lowest Energy Trimer **Lowest Energy Dimer**

Figure 7. Lowest energy dimer, trimer, and tetramer structures of **2**. The molecular numbering corresponds to that shown for the heptamer in Figure 4. The dimer is a herringbone structure, whereas the trimer and tetramer are pinwheel-like structures.

Tables 3 and 4 show the results of these simulations for each crystal. For **3** the lowest energy stage 1 chain has glide symmetry with a repeat vector of 8.126 Å along the unit cell *a*-axis as shown in Figure 6b. The carboxyl hydrogens do not hydrogen bond in this stage (the H-bond energy in Table 3, column 3, is 0 for this stage). **2**, on the other hand, has a stage 0 dimer structure, as seen in Figure 7. The two molecules are unrelated by any symmetry element, and there is no H-bond between them. This dimer was then used to find the lowest energy chain, a translation chain of dimers shown in Figure 6a

Lowest Energy Heptamer

Figure 8. The lowest energy heptamer structure extracted from the layer of **2**. Oxygen atoms in red.

TABLE 5: Lowest Energy Clusters in 2

cluster type	average energy[a]
dimer	−5.46
trimer	−9.57
tetramer	−11.90
heptamer	−16.08
layer[b]	−30.25

[a] Average energy per molecule in kcal/mol evaluated for the cluster using eqs 1 and 2. [b] Stage 2 energy from Table 4.

with a repeat vector of 7.082 Å along the unit cell *a*-axis. Comparison of parts a and b of Figure 6 of the two chains shows their strong structural similarity. The chain in Figure 6b is a true glide chain, while that in Figure 6a is a pseudoglide chain.

Stage 2 structures for each molecule are shown in Figure 4. The structure for **2** (Figure 4a) is a translation layer of dimers, whereas that for **3** is a true glide layer. As indicated by Tables 3 and 4 for this stage, there is still no hydrogen bond present. Again, as for the chains, the two layers look structurally very similar. The repeat vectors for the pseudoglide layer of **2** lie along the *a* and *b* unit cell axis (7.082 and 7.660 Å, respectively) with an angle of 98.90° between them. The stilbene units are tilted 41.18° with respect to the layer normal. The repeat vectors for the true glide layer of **3** also lie along the *a* and *b* unit axes (8.126 and 7.467 Å, respectively) with an angle of 90.00°. The tilt angle of the stilbenes in this layer is 48.22° with respect to the layer normal, similar to the layer for **2**.

The vector nature of the hydrogen bond first occurs in the stage 3 interlayer through the inversion coupling of the layers from stage 2. This is indicated in Tables 3 and 4 by the large positive repulsive values of the H-bond van der Waals energy (+4.96 kcal for **3** and +6.02 kcal for **2**) as the donor H atoms approach the acceptor O atoms across the inversion. Comparison of the energies for stage 2 and stage 3 shows that the crystal lattice energy is very anisotropic with 76% of the energy for **2** and 71% of that for **3** already appearing within the lattice of the "monolayer" (for an isotropic lattice this would be 50%). The last row of the tables indicates that most of the energy for binding the layers together is electrostatic in nature, resulting from the hydrogen bonding, whereas most of the energy for binding the chains together to make the individual layers is nonbonded van der Waals coupling. The similarity of the two layer structures is thus not surprising; they differ by only the nonbonded interaction of one methylene group.

The crystal structure of **2** has also been analyzed for the packing energy and geometry of small clusters. The lowest energy dimer, trimer, tetramer, and heptamer were determined by evaluating eqs 1 and 2 for various clusters of differing geometry. The average energy of a molecule (in kcal/mol) in the cluster was computed by dividing the total cluster energy by the number of molecules. The results are shown in Figures 7 and 8 and in Table 5. As the cluster grows, the energy approaches the layer lattice energy. The dimer has the typical herringbone or T-shape pattern so often seen in aromatic ring systems such as the benzene dimer. The trimer, tetramer, and heptamer have the pinwheel-like geometry previously suggested to occur in phospholipid vesicles of the SFAs and related phospholipids and other aromatics and dyes such as the squaraines. These chiral structures can account for the observed induced circular dichroism spectra when the unit aggregates are generated in the presence of a chiral host.[6,10,21] The intriguing differences in fluorescence (Figure 5) for the crystals appear to be correlated (λ_{max} increases with decrease in the repeat distance along the *b* unit axis, Table 2) with the "tightness" of the unit tetramer, although more structures would be needed to establish any clear trends or conclusions. The structures of the layers in **1** and **5** are almost identical; this together with energy calculations and similarities in structure to *trans*-stilbene indicates that the main interaction in the crystal is indeed the aromatic−aromatic interaction and that the carboxylic hydrogen bonding plays no role in the structure of a single layer.

In summary, the crystal structures obtained for **1**−**3** and **5** provide remarkable support for the structure of the "unit aggregates" deduced and simulated for stilbene, azobenzene, and tolan derivatives and suggest that these species may be the key intermediates in the formation of crystals and microcrystals. The close agreement between spectroscopic properties of the "extended arrays" of LB films and the crystals and the isolated "unit aggregates" in solution, considered together with the calculated interaction energies from the crystal structures, reinforces the idea that the strongest intermolecular interactions occur within these clusters and that these are true supramolecular species.

Acknowledgment. We are grateful to the National Science Foundation (Grant CH-86-16361) for support of this research. We also thank Prof. W. D. Jones for his help in operating the X-ray diffractometer and the Center for Photoinduced Charge Transfer for supporting J.P.

Appendix

Energetic Analysis of the Crystal Structure. To carry out the analysis, each molecule was packed in its respective space group with sufficient unit cell repetitions so that at least one asymmetric unit (the packing unit) was completely surrounded by other molecules. CHEMX was found extremely useful for this purpose, as the molecules of different symmetry could be distinguished by coloring them. In addition the software for computing the interaction potential could be easily interfaced

to CHEMX using the CHEMLIB software development tools.[22] The interaction potential between the packing unit and all the other molecules was then computed using the nonbonded and electrostatic terms of the CFF91 force field given by eqs 1 and 2. The lattice energy for each stage was then computed using eq 3.

$$E^{\mathrm{nb}} = \sum_{i,j} A_{ij}\left[2\left(\frac{B_{ij}}{r_{ij}}\right)^9 - 3\left(\frac{B_{ij}}{r_{ij}}\right)^6\right] \quad (1)$$

$$E^{\mathrm{el}} = \sum_{i,j} \frac{q_i q_j}{\epsilon_0 r_{ij}} \quad (2)$$

$$E_{\mathrm{lattice}} = (1/2)(E^{\mathrm{nb}} + E^{\mathrm{el}}) \quad (3)$$

In eq 1 E^{nb} is the nonbonded van der Waals dispersive and repulsive term with parameters A_{ij} and B_{ij} given by the force field, and r_{ij} is the atom−atom distance. In eq 2 E^{el} is the Coulomb electrostatic term with a dielectric constant $\epsilon_0 = 1.0$. The summation in eqs 1 and 2 is over all atoms, *i*, in the packing unit interacting with all atoms, *j*, in all the other molecules of the crystal. The partial atomic charges, *q*, in eq 2 are those given by the force field. Interestingly, the presence of H-bonding in any KAP stage becomes readily apparent by extracting the H atom contribution to eq 1. We make the following assertion about the presence of H-bonding.

For H atom donors (O or N) in the packing unit, E^{nb} for the hydrogen atom is always greater than 0 if the donor is involved in a hydrogen bond and less than or equal to 0 otherwise.

In another paper this is demonstrated with several examples.[23] In the current case, for both **2** and **3**, E^{nb} for the donor hydrogen on the carboxyl group is only greater than 0 in stage 3 of KAP. We represent this as a type 1_3 hydrogen bond. In this notation type 1 refers to the fact that the hydrogen bond only occurs in a single KAP stage and the subscript indicates which one. There are 16 H-bond types, which are detailed elsewhere.[23]

The lattice energy of each stage is finally given by eq 3, where the 1/2 is inserted to avoid double counting of the energy. If the packing unit contains more than one molecule, then the lattice energy is computed by adding the energy of the packing unit (stage 0 energy different from 0) to eq 3 and then dividing by the number of molecules in the packing unit (for **2**, this means dividing by 2).

Supporting Information Available: Atomic coordinates for all atoms, bond lengths, and angles, anisotropic displacement parameters, torsion angles, and least-squares planes (39 pages). Ordering information is given on any current masthead page.

References and Notes

(1) Kuhn, H. In *Light Induced Charge Separation in Biology and Chemistry*; Gerischer, H., Katz, J. J., Eds.; Dahlem Konferenzen: West Berlin, 1979; pp 151−169.

(2) Gilman, P. B. In *Photographic Sensitivity*; Cox, R. J., Ed.; Academic Press: London, 1973; p 187.

(3) Sturmer, D. M. In *Special Topics in Heterocyclic Chemistry*; Weissburger, A., Taylor, E. C., Eds.; Wiley: New York, 1977; p 540.

(4) Furman, I.; Geiger, H. C.; Whitten, D. G.; Penner, T. L.; Ulman, A. *Langmuir* **1994**, *10*, 837−843.

(5) Song, X.; Geiger, C.; Furman, I.; Whitten, D. G. *J. Am. Chem. Soc*. **1994**, *116*, 4103−4104.

(6) Song, X.; Perlstein, J.; Whitten, D. G. *J. Am. Chem. Soc*. **1995**, *117*, 7816.

(7) Chen, H.; Law, K. Y.; Perlstein, J.; Whitten, D. G. *J. Phys. Chem*. **1994**, *98*, 5138.

(8) Farahat, C. W.; Penner, T. L.; Ulman, A.; Whitten, D. G. *J. Phys. Chem*. **1996**, *100*, 12616.

(9) Geiger, C. Unpublished results.

(10) Chen, H.; Farahat, M.; Law, K. Y.; Whitten, D. G. *J. Am. Chem. Soc*. **1996**, *118*, 2584.

(11) Walker, N.; Stuart, D. *Acta Crystallogr*. **1983**, *A29*, 158−166.

(12) Cromer, D. T.; Waber, J. T. *International Tables for X-ray Crystallography*; The Kynoch Press: Birmingham, England, 1974; Vol. IV, Table 2.2 A.

(13) Cromer, D. T. *International Tables for X-ray Crystallography*; The Kynoch Press: Birmingham, England, 1974; Vol. IV, Table 2.3.1.

(14) TEXSAN-TEXRAY Structure Analysis Package. Molecular Structure Corporation, 1985.

(15) Spooner, S. P. Ph.D. Thesis, University of Rochester, 1993.

(16) Finder, C. J.; Newton, M. G.; Allinger, N. L. *Acta Crystallogr*. **1974**, *B30*, 411.

(17) Song, X.; Geiger, C.; Leinhos, U.; Perlstein, J.; Whitten, D. *J. Am. Chem. Soc*. **1994**, *116*, 10340.

(18) Kitaigorodskii, A. I. *Organic Chemical Crystallography*; Consultants Bureau: New York, 1961. Chapter 3, pp 65−112.

(19) (a) Hwang, M. J.; Stockfisch, T. P.; Hagler, A. T. *J. Am. Chem. Soc*. **1994**, *116*, 2515−2525. (b) Maple, J. R.; Hwang, M.-J.; Stockfisch, T. P.; Dinur, U.; Waldman, M.; Ewig, C. S.; Hagler, A. T. *J. Comput. Chem*. **1994**, *15*, 162−182. (c) *Discover User Guide, Version 2.8 Part 2*; Biosym Technologies, San Diego, March 1992. A complete set of parameters for the CFF91 force field are listed in this version.

(20) (a) Perlstein, J. *J. Am. Chem. Soc*. **1994**, *116*, 11420. (b) Perlstein, J. *J. Am. Chem. Soc*. **1994**, *116*, 455.

(21) Chen, H.; Law, K. Y.; Perlstein, J.; Whitten, D. G. *J. Am. Chem. Soc*. **1995**, *117*, 7257−7258.

(22) CHEM-X is a molecular modeling program developed and distributed by Chemical Design Ltd., Roundway House, Cromwell Park, Chipping Norton, Oxfordshire OX7 5SR, U.K. CHEMLIB is a CHEMX interface that allows the user to link his own subroutines to CHEMX.

(23) Perlstein, J.; Steppe, K.; Vaday, S.; Ndip, E. M. *J. Am. Chem. Soc*. **1996**, *118*, 8433.